COMPEL—The International Journal for Computation and Mathematics in Electrical and Electronic Engineering
Vol. 3, No. 2, 79–105 © 1984 BOOLE PRESS LIMITED

ON MODELING THE INTRINSIC NUMBER AND FERMI LEVELS FOR DEVICE AND PROCESS SIMULATION

W. JÜNGLING, E. GUERRERO and S. SELBERHERR
Institut für Allgemeine Elektrotechnik und Elektronik, Abteilung Physikalische Elektronik, TU Wien, Gußhausstr. 27, A-1040 Wien, Austria

ABSTRACT: We discuss three models describing the carrier densities in highly doped silicon, which have been used for process and device simulation. We calculate n_{ie} for each of the models for various doping concentrations within temperature ranges interesting for the device and process simulation. We try to explain the behaviour of n_{ie} for high compensation and compare our calculated results to measured values of n_{ie}. We offer simple formulae for the calculated n_{ie} and show how far the relations between the carrier densities and the Fermi levels can be described by the simple formulae of Boltzmann statistics when we use a doping dependent effective intrinsic number.

NOTATION

a	l Lattice constant of silicon, cm
ε	p Permittivity of silicon, $eV^{-1}\,cm^{-1}$
$D_{n,p}$	d Diffusion coefficient of electrons/holes, $cm^{-2}\,s^{-1}$
E	energy, eV
$E_{A,D}$	energy level of the acceptor or donor atoms, eV
E_G	bandgap, eV
F	Fermi energy, eV
F_n	quasi-Fermi energy of electrons, eV
F_p	quasi-Fermi energy of holes, eV
φ_n	quasi-Fermi level of electrons, V
φ_p	quasi-Fermi level of holes, V
h	Planck's constant/2π, eV s
k	Boltzmann's constant, $eV\,K^{-1}$
$L_{n,p}$	d Diffusion length of electrons/holes, cm
λ	screening length, cm
λ_D	Debye length, cm
m_0	electron mass, $eV\,cm^{-2}\,s^{-2}$
m_n	relative mass of the electrons, 1
m_p	relative mass of the holes, 1
n	electron density, cm^{-3}
p	hole density, cm^{-3}
n_{ie}	effective intrinsic carrier density, cm^{-3}
$N_{A^{(-)}_{(+)}}$	density of (ionised) acceptors, cm^{-3}
N_D	density of (ionised) donators, cm^{-3}
q	charge unit, e

$\rho_{A,D}$	densities of states of the impurity atoms, $cm^{-3}\,e^{-1}\,V^{-1}$
$\rho_{c,v}$	densities of states in silicon, $cm^{-3}\,e^{-1}\,V^{-1}$
σ	standard deviation, eV
σ_e	effective standard deviation, eV
T	temperature, K

1. INTRODUCTION

At low doping concentrations the intrinsic number is only temperature dependent whereas at higher concentrations pn becomes also doping dependent. This phenomenon has been proved by optical and electrical measurements as well as by theoretical calculations. Various experiments and theoretical investigations have been undertaken to work out quantitative values for the increase of the effective intrinsic number. Both measurements and theoretical approaches contain several uncertainties, some of which are discussed here.

Experimental data of n_{ie} are measured as a function of the free carriers and not the impurity concentration as it is often assumed. Slotboom and De Graaf [1] and Wieder [2] have derived values of $D_p np$ and $D_n np$ by measurements of the $I_C(U_{BE})$ characteristic of bipolar transistors with an homogeneous highly doped base. These measurements contain the uncertainties of the base width, the base concentration and especially the minority diffusion coefficient D_p in heavily doped material. Mertens and Van Overstraeten [3] have developed a new technique to measure $n_{ie}^2 D_p/L_p$, $n_{ie}^2 L_p$ and L_p simultaneously to obtain more accurate results. Further methods to measure the effective intrinsic carrier density and minority current parameters have been developed by Lindholm et al. [4] for shallow emitters and by Possin et al. [5] based on epitaxial bipolar transistors.

Difficulties appear when the measured values of n_{ie} are used in the current relations for device simulation. The measurement of the effective intrinsic carrier densities offers no information about the relations between the carrier densities and the quasi-Fermi levels in the semiconductor. In, for example, ref. [5] the uncertainty about degeneracy and the exact shrinkage of the valence and the conduction band is compensated by an additional term in the electrical field to describe the minority current correctly. As Boltzmann statistics may only be used in moderately doped semiconductors, theoretical models describing highly doped silicon are necessary to examine the validity of the concept of a doping dependent bandgap (or an effective intrinsic number) together with Boltzmann statistics.

If the results of measurements do not differ gravely from the theoretical values, the validity ranges of the theoretical models could also be used for the measured values of the effective intrinsic number.

This work gives a survey of three theoretical models describing the densities-of-states in highly doped silicon. The models are derived by theoretical investigations of Bonch-Bruevich [6], Morgan [7] and Kane [8] and have been used by Van Overstraeten et al. [9], Jain and Van Overstraeten [10], Slotboom [11], Mock [12], Nakagawa [13] and Polsky and Rimshans [14] for process and device simulation. Charge neutrality and thermodynamic equilibrium are assumed in our calculations of n, p and F. Therefore differences of the models will mainly affect the minority carrier densities and the Fermi levels. Hence, the effective intrinsic number, defined by $n_{ie}^2 := np$ is estimated to be a good parameter to compare different models. As n_{ie}

can be measured by various methods it offers the possibility to compare the calculated results to measured values. n_{ie} influences the diffusion constants for the impurity atoms at high temperatures. Therefore, we can expect different results of process simulations when using a doping dependent n_{ie} instead of the usually taken, only temperature dependent, n_{ie} of Morin and Maita [15]. These results may be used to prove the validity of the theories at diffusion temperatures.

The calculated values of n_{ie} show remarkable minima for strongly compensated silicon. We attempt to find a physical explanation for the behaviour of n_{ie} and calculate characteristic parameters of the models for uncompensated and for strongly compensated silicon at 300 K.

The evaluation of the theoretical models is very difficult and extensive in terms of computer time. Therefore, we are looking for a simple method to implement the models into existing programs. For 300 K temperature we examine how far Boltzmann statistics can describe the relations between the quasi-Fermi energies and the carrier densities using doping dependent intrinsic carrier densities. The validity range is checked by comparison of the quasi-Fermi energies. As a result of these investigations we receive maximal concentrations limiting the validity range of the classical relations between n and F_n or p and F_p. We believe that these doping limits may also be used for effective intrinsic numbers derived from measurements. Therefore, the approximation of measured or calculated values of n_{ie} by simple formulae is only interesting up to these doping concentrations. Beyond these concentrations neither a doping dependent bandgap nor an effective intrinsic number can describe the Fermi levels and the minority carrier densities exactly.

For 275–400 K temperature we offer simple formulae of n_{ie} for all three models when only one dopant species is present.

For Van Overstraeten's model we have constructed more complicated formulae which evaluate n_{ie} for low and high concentrations for uncompensated as well as for strongly compensated material within temperature ranges 275–400 K and 800–1200°C.

These approximations can be used to implement the model into existing programs and examine how the results of process and device simulations are affected by the "absolute value" of $[N_D - N_A] > 10^{17}\,\mathrm{cm}^{-3}$.

2. THE MODELS

The formulae of Van Overstraeten's model (index "ov") are well described in [9] and [10], the formulae of Slotboom's model (index "sl") have been derived from [11] and Mock's model (index "mo") is defined in [12]. These three models obtain the total densities-of-states as the envelope of the impurity band and the valence or conduction band which differs from the models by Kleppinger and Lindholm [16] which assume the total densities-of-states to be the sum of the two bands. The modeling of the relative masses and the bandgap has been taken from [17] for the low temperature range (275–400 K) and from [10] for the high temperature range (800–1200°C). Furthermore, we assume total ionisation of the impurity atoms ($N_A^- = N_A$ and $N_D^+ = N_D$). No limitations of the validity range have been published for Slotboom's and Mock's models, whereas Van Overstraeten's model is only valid for "absolute value" $[N_D - N_A] > 10^{17}\,\mathrm{cm}^{-3}$.

We set the energy to zero in the middle of the forbidden band and count F_n and E

positive in direction to the conduction band for the calculation of n. F_p and E are positive in direction to the valence band for the calculation of p.

The following formulae describe the different models. If the equations have no index, they are valid for each of the three models.

$$n = \int_{-\infty}^{+\infty} \max\left(\frac{\rho_c(E), \rho_D(E)}{1+\exp(E-F_n)/kT}\right) dE \tag{1}$$

$$p = \int_{-\infty}^{+\infty} \max\left(\frac{\rho_v(E), \rho_A(E)}{1+\exp(E-F_p)/kT}\right) dE \tag{2}$$

$$F_n = q(\Psi - \varphi_n) \tag{3}$$

$$F_p = q(\varphi_p - \Psi) \tag{4}$$

The authors model the screening length in different ways. In refs. [9], [11] and [12] the screening lengths are given, respectively, as

$$\lambda^{-1} = 0.5599(m_0 m_{n,p}/\varepsilon)^{1/2}(q/h)[N_D - N_A]^{1/6} \tag{5 ov}$$

$$\varepsilon\lambda^{-2} = q^2(\partial n/\partial F_n + \partial p/\partial F_p) \tag{5 sl}$$

$$\varepsilon\lambda^{-2} = q^2(\partial n/\partial F_n + \partial p/\partial F_p + (N_D + N_A)/30kT) \tag{5 mo}$$

The densities-of-states for the conduction band or valence band are defined by

$$\sigma = q^2\left(\frac{\lambda(N_A + N_D)}{8\pi\varepsilon^2}\right)^{1/2} \tag{6 ov, sl}$$

$$\sigma = q^2\left(\frac{\lambda(N_A + N_D)}{8\pi\varepsilon^2}\right)^{1/2} \exp\left(-\frac{0.5a}{\lambda}\right) \tag{6 mo}$$

$$y(x) = \pi^{-1/2} \int_{-\infty}^{x} (x-u)^{1/2} \exp(-u^2)\, du \tag{7}$$

$$\rho_{c,v}(E) = (m_0 m_{n,p})^{3/2}(2^{3/2}\sigma)^{1/2}\pi^{-2}h^{-3} y \frac{(E - E_G/2)}{\sqrt{2}\sigma} \tag{8}$$

Figure 1 shows the shape of $y(x)$ in the interval $-2 < x < +2$ in comparison with the classical $x^{1/2}$ model for the densities-of-states in silicon. Figure 1 helps to estimate the band structure in silicon. The temperature dependent band edge lies at $x = 0$, the value of $x = -1$ lies $\sqrt{2}\sigma$ eV deep in the forbidden gap. (Values for $\sqrt{2}\sigma$ can be derived from Figs. 13 and 14.)

The densities-of-states of the impurity atoms are given by

$$\sigma_e = 1.03\left(\frac{q^2[\lambda(N_A + N_D)]}{8\pi\varepsilon^2}\right)^{1/2} \exp\{-[11.3806\pi(N_A + N_D)]^{-1/2}\lambda^{-3/2}\} \tag{9}$$

$$\rho_{A,D} = 2N_{A,D}(2\pi\sigma_e^2)^{-1/2} \exp(-(E - E_{A,D})^2/2\sigma_e^2)\,. \tag{10}$$

For the temperature range 275–400 K we set

$$E_G = 1.1785 - 9.025 \times 10^{-5} T - 3.050 \times 10^{-7} T^2 \tag{11a}$$

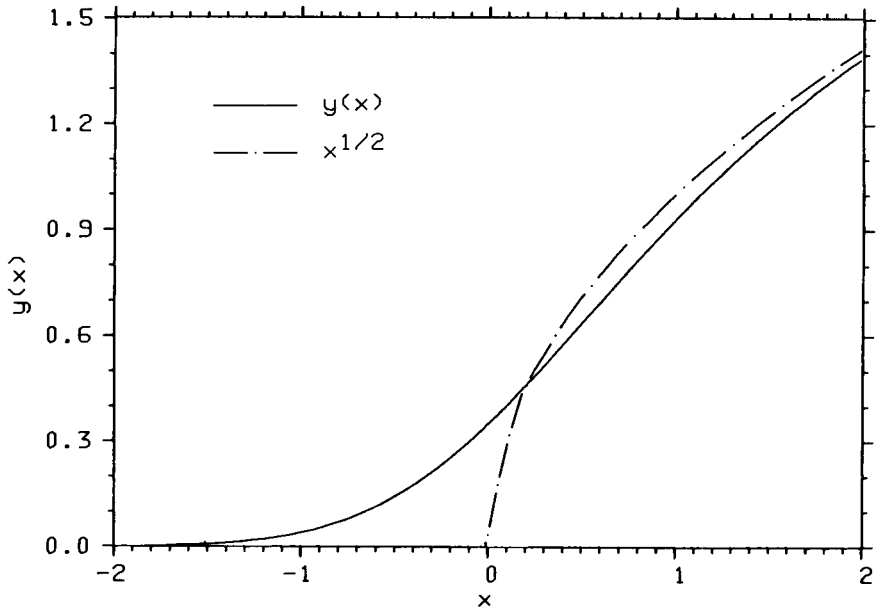

Fig. 1. $y(x)$ (——) describing the densities of states in highly doped silicon in comparison with the classical $x^{1/2}$ formula (– – –).

$$m_n = 1.045 + 4.500 \times 10^{-4} T \tag{12a}$$

$$m_p = 0.523 + 1.400 \times 10^{-3} T - 1.480 \times 10^{-6} T^2 \tag{13a}$$

for the temperature range 800–1200°C we use

$$E_G = 1.205 - 2.8 \times 10^{-4} \tag{11b}$$

$$m_n = (1.1925 E_G / E_G(T))^{2/3} \tag{12b}$$

$$m_p = (0.67818 E_G / E_G(T))^{2/3} \tag{13b}$$

The ionisation energies of donors and acceptors are set to 0.044 eV for boron and phosphorus counted from the valence and the conduction band edge, respectively. Furthermore, we assume that the ionisation energies are temperature independent.

3. THE CALCULATION OF THE INTRINSIC NUMBER

Thermodynamic equilibrium and charge neutrality are assumed for the calculation of the effective intrinsic carrier densities $n_{ie}^2 := np$, i.e. $F = +F_n = -F_p$ and $n(F_n) - p(F_p) = N_D^+ - N_A^-$. The programs which evaluate $n = n(T, N_D, N_A, F_n, \lambda)$ and $p = p(T, N_A, N_D, F_p, \lambda)$ are taken from [18]. In appendix A we point out how eqs. (1)–(13) have been solved and how the error of the calculation can be estimated.

We evaluate n, p and F by Newton iterations in F for Van Overstraeten's model. The evaluation of Slotboom's and Mock's models is more difficult, because λ_0, the screening length which is used to evaluate carrier densities n and p, must be identical

to λ_1, the screening length defined by (5 sl) and (5 mo). We have to evaluate a λ_0 that equals the relation

$$\lambda_1 = \lambda_1(N_D, N_A, \partial n/\partial F_n, \partial p/\partial F_p, \lambda_0) = \lambda_0$$

This leads to fixpoint iterations in λ as well as to Newton iterations in F. Calculations have shown that Banach fixpoint iterations do not converge for the low temperature range. Therefore, we use the improved fixpoint method by Aitken, which is given in appendix B.

The intrinsic number is calculated for n-doped silicon. We have calculated n_{ie} as a function of the doping difference and take N_A as a parameter to get a survey of lightly and heavily doped silicon with, as well as without, compensation.

4. RESULTS

In Figs. 2–10 we present the results of our calculations in n-doped silicon. In some figures $n_{ie,ov}$ is evaluated for doping differences less than 10^{17} cm^{-3} in order to be able to compare the results more easily. The parameter in Figs. 2–10 is the doping concentration of the acceptors. The plotted lines have numbers which indicate the value of N_A with respect to the following table.

1 ..... 10^{10} cm^{-3}	2 ..... 10^{16} cm^{-3}
3 ... 3.16×10^{16} cm^{-3}	4 ..... 10^{17} cm^{-3}
5 ... 3.16×10^{17} cm^{-3}	6 ..... 10^{18} cm^{-3}
7 ... 3.16×10^{18} cm^{-3}	8 ..... 10^{19} cm^{-3}
9 ... 3.16×10^{19} cm^{-3}	10 ..... 10^{20} cm^{-3}
11 ... 3.16×10^{20} cm^{-3}	12 ..... 10^{21} cm^{-3}
13 ... 3.16×10^{21} cm^{-3}	

Figures 2–7 show the results for the temperature range significant for device simulation.

Van Overstraeten's model (Figs. 2 and 5) predicts the largest values for the intrinsic number at high doping concentrations. For strongly compensated silicon $n_{ie,ov}$ increases weaker than $n_{ie,sl}$. For high acceptor concentrations minima occur for $N_D - N_A = 0.5(N_A + N_D)$.

Slotboom's model (Figs. 3 and 6) shows remarkable minima for $N_D - N_A = 0.5(N_A + N_D)$. The calculated results can be divided into a saturation region (left upper part of the figures), where $n_{ie,sl}$ is independent from the doping difference; a region where $n_{ie,sl}$ decreases for increasing doping differences; and a region of uncompensated silicon, where $n_{ie,sl}$ increases with increasing doping concentrations. $n_{ie,sl}$ is a lower value than $n_{ie,ov}$ for highly doped silicon without compensation, which is a result of the different modeling of the screening length. It seems remarkable that in strongly compensated silicon $n_{ie,sl}$ is larger than in highly doped uncompensated material.

$$n_{ie,sl}(N_D = 1.01 \times 10^{20}\ \text{cm}^{-3}, N_A = 10^{20}\ \text{cm}^{-3}) > n_{ie,sl}(N_D = 10^{22}\ \text{cm}^{-3})$$

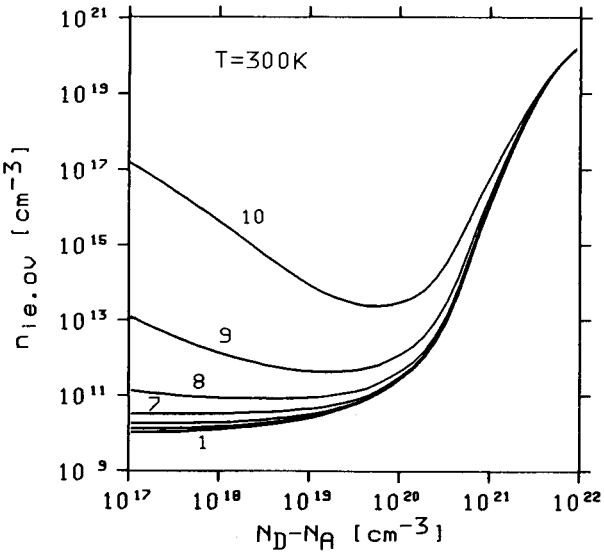

Fig. 2. The intrinsic number calculated by Van Overstraeten's model at 300 K in n-doped silicon for various acceptor concentrations.

Mock's model (Figs. 4 and 7) predicts the lowest values for n_{ie} which can be related from the modeling of the standard deviation σ. For strongly compensated material the behaviour of $n_{ie,mo}$ is similar to $n_{ie,sl}$. $n_{ie,mo}$ shows a saturation region, a region of decreasing and a region of increasing n_{ie}. For uncompensated material $n_{ie,mo}$ increases far more slowly with the doping concentration than $n_{ie,ov}$ or $n_{ie,sl}$. It is

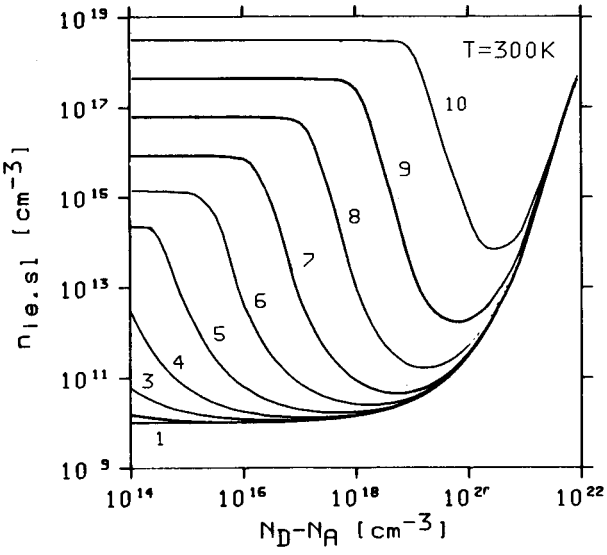

Fig. 3. The intrinsic number calculated by Slotboom's model at 300 K in n-doped silicon for various acceptor concentrations.

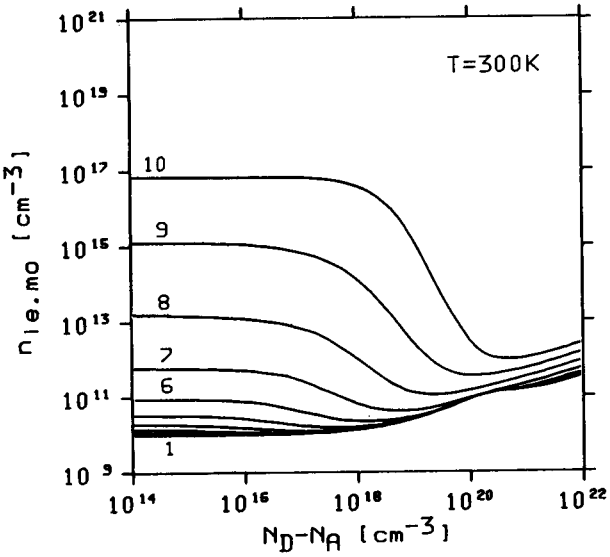

Fig. 4. The intrinsic number calculated by Mock's model at 300 K in n-doped silicon for various acceptor concentrations.

remarkable that the intrinsic number of this model is about 10^3 times larger in strongly compensated material than in highly doped uncompensated material although the total doping concentration of the uncompensated silicon is about 100 times larger than the total doping concentration of the compensated silicon.

Figures 5–7 show the temperature dependence of the intrinsic number in the low temperature range for various doping concentrations. For strongly compensated

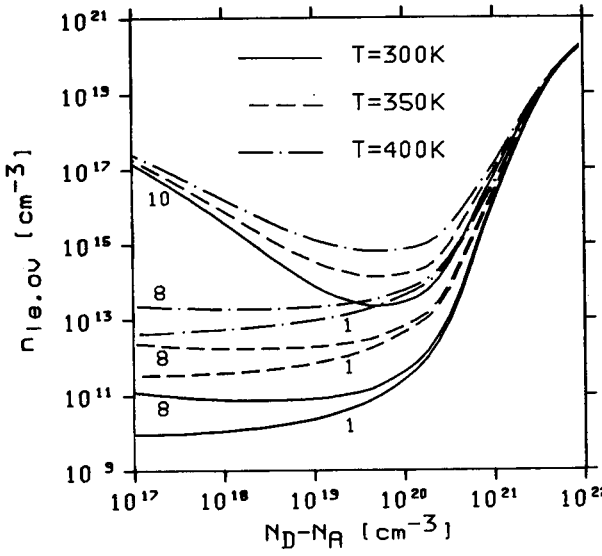

Fig. 5. The intrinsic number calculated by Van Overstraeten's model for 300 K (——), 350 K (– – –) and 400 K (–·–·–) for $N_A = 10^{10}$ cm^{-3}, 10^{19} cm^{-3} and 10^{20} cm^{-3}.

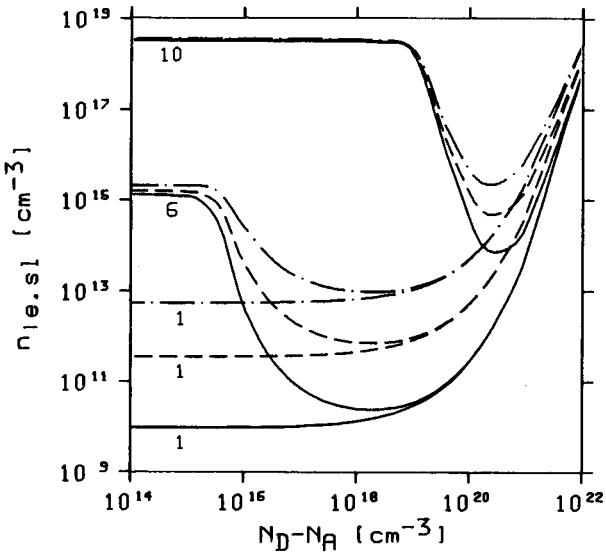

Fig. 6. The intrinsic number calculated by Slotboom's model for 300 K (——), 350 K (– – –) and 400 K (–·–·–) for $N_A = 10^{10}$ cm^{-3}, 10^{18} cm^{-3} and 10^{20} cm^{-3}.

material and very high doped uncompensated material n_{ie} shows only a weak temperature dependence, whereas the temperature dependence increases for low doping concentrations and for concentrations where n_{ie} shows minima.

For the temperature range 800–1200°C (Figs. 8–10) n_{ie} shows qualitatively the same shapes as in low temperature range. Affected by the higher value of the temperature dependent intrinsic number all plotted curves occur smoother and

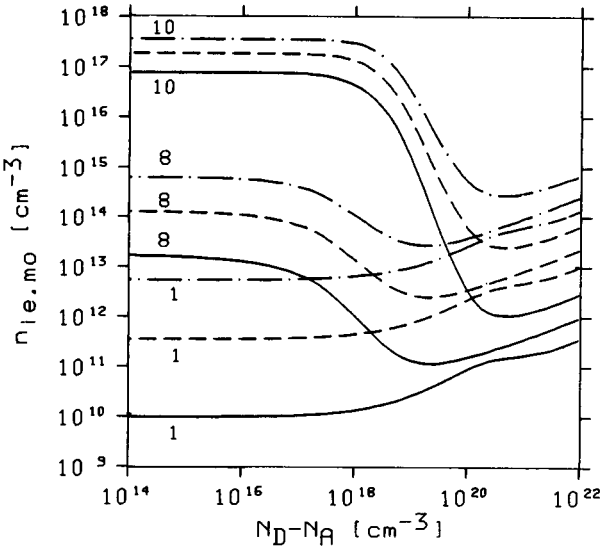

Fig. 7. The intrinsic number calculated by Mock's model for 300 K (——), 350 K (– – –) and 400 K (–·–·–) for $N_A = 10^{10}$ cm^{-3}, 10^{19} cm^{-3} and 10^{20} cm^{-3}.

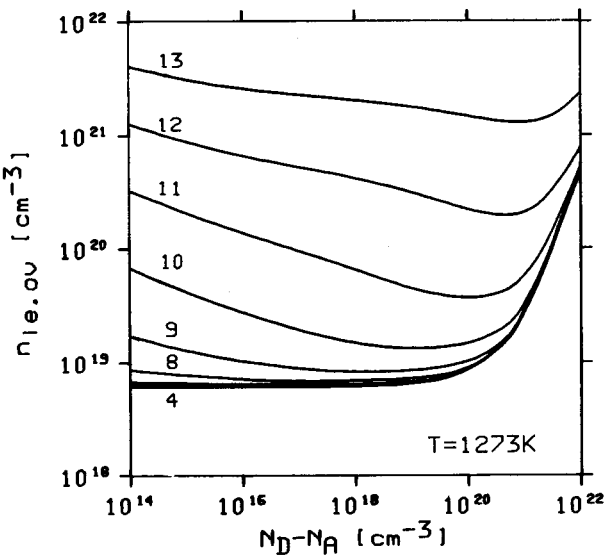

Fig. 8. The intrinsic number calculated by Van Overstraeten's model at 1000°C in n-doped silicon for various acceptor concentrations.

"damped". For low doping concentrations the calculated n_{ie} agrees with the formula of Morin and Maita which has also been pointed out in [10].

5. DISCUSSION OF λ, σ AND σ_e

The calculated results of n_{ie} show that $n_{ie,ov} > n_{ie,sl} > n_{ie,mo}$ and predict minima for

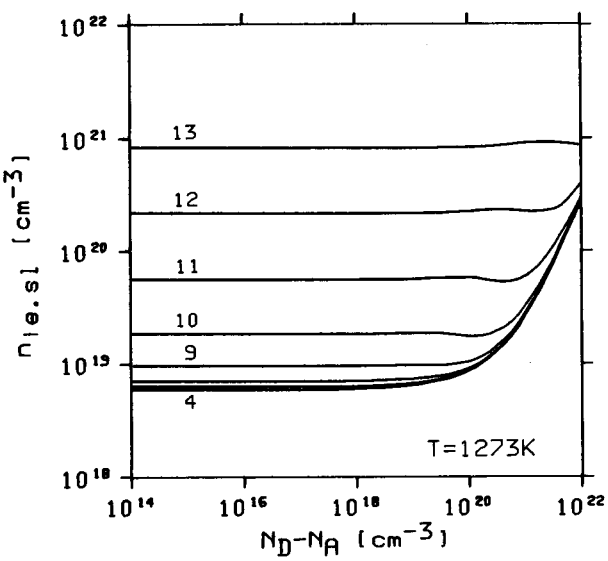

Fig. 9. The intrinsic number calculated by Slotboom's model at 1000°C in n-doped silicon for various acceptor concentrations.

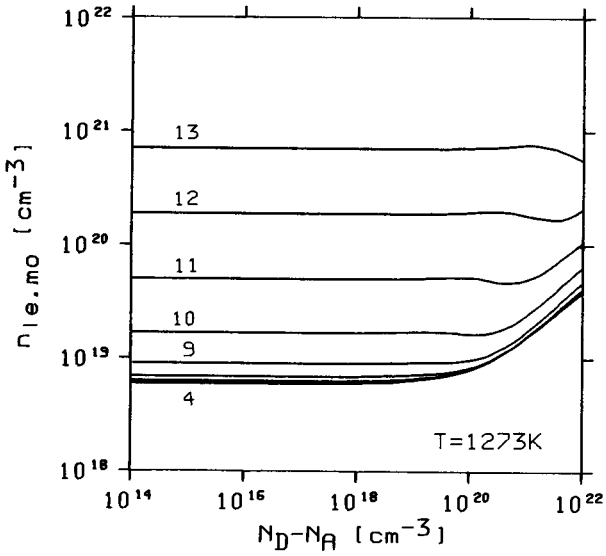

Fig. 10. The intrinsic number calculated by Mock's model at 1000°C in n-doped silicon for various acceptor concentrations.

all models for $N_D - N_A = 0.5(N_A + N_D)$. We attempt to give a physical explanation for these characteristics and try to reduce them to the behaviour of λ, σ and σ_e. The screening lengths decrease with the increasing number of free carriers which screen perturbations of the potential in the semiconductor.

For uncompensated silicon Figs. 11, 13 and 15 show the values of λ, σ and σ_e, respectively. For low doped silicon, the value of λ_{sl} and λ_{mo} coincide with the Debye length λ_D. For higher doping concentrations the screening lengths evaluate higher values, which is an effect of Fermi statistics ($\partial n/\partial F_n < n/(kT)$). λ_{ov} has been derived from the Fermi model for degenerated semiconductors and is only valid when the quasi-Fermi energy enters the valence or conduction band. It can hardly be compared with the other screening lengths. At higher concentrations the impurity atoms influence the band structures which results in increasing values of the standard deviation σ. σ_{ov} and σ_{sl} increase monotonously with the doping concentration whereas σ_{mo}, influenced by the factor $\exp(-0.5a/\lambda)$, increases weaker up to doping concentrations of 3×10^{20} cm^{-3} and decreases for higher concentrations. $\sigma_{e,sl}$ and $\sigma_{e,mo}$ are similar which indicates that the screening length is the dominant parameter for σ_e.

For strongly compensated material λ, σ and σ_e are plotted in Figs. 12, 14 and 16, respectively. λ_{sl} and λ_{mo} are constant for very high compensation but then fall with increasing doping difference similar to the Debye length. λ_{ov} differs significantly from the other screening lengths and is hard to compare. The standard deviation shows minima like the intrinsic carrier densities. Figures 12 and 14 can be divided into three parts. In the left part λ and the total carrier density are constant and, therefore, σ as well. For these doping concentrations we find a great number of impurity atoms but only few electrons in the semiconductor so that the potential perturbations of the impurity atoms cannot be screened efficiently. Therefore, σ has a large value which indicates the strong effect of the impurity atoms on the

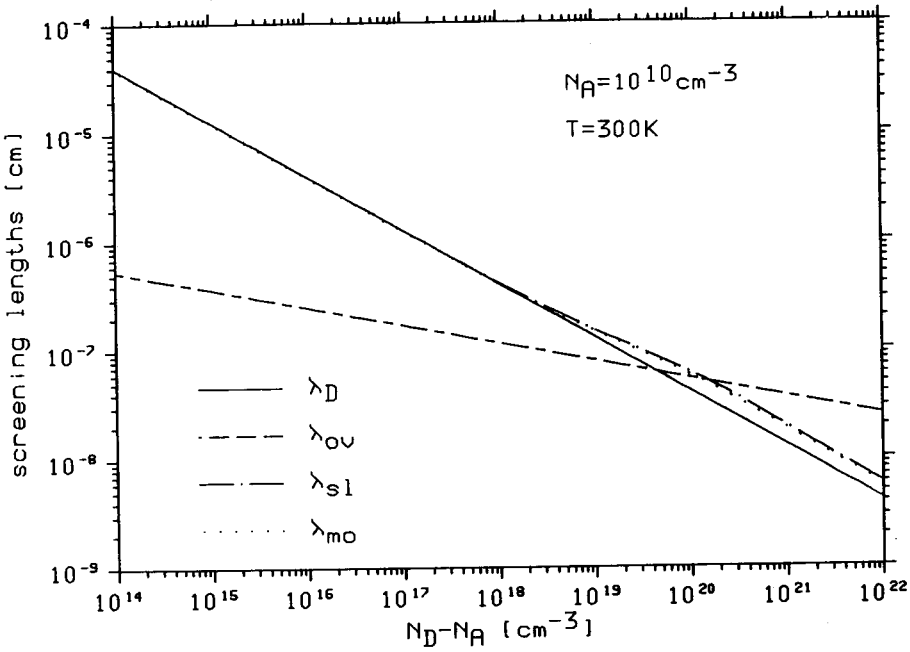

Fig. 11. Various screening lengths for n-doped silicon at 300 K for uncompensated n-silicon ($N_A = 10^{10}\,cm^{-3}$).

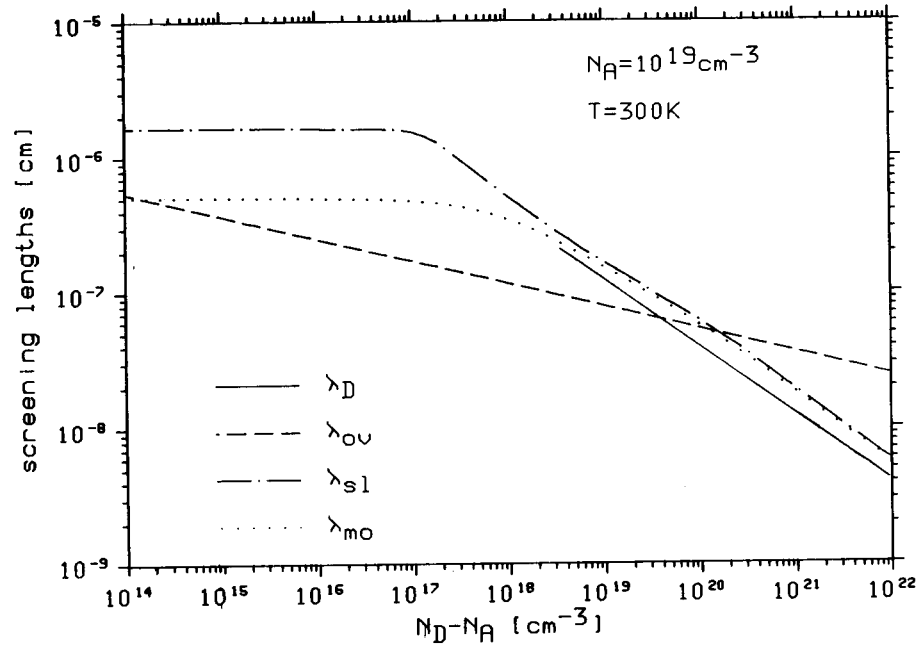

Fig. 12. Various screening lengths at 300 K for strongly compensated n-silicon ($N_A = 10^{19}\,cm^{-3}$).

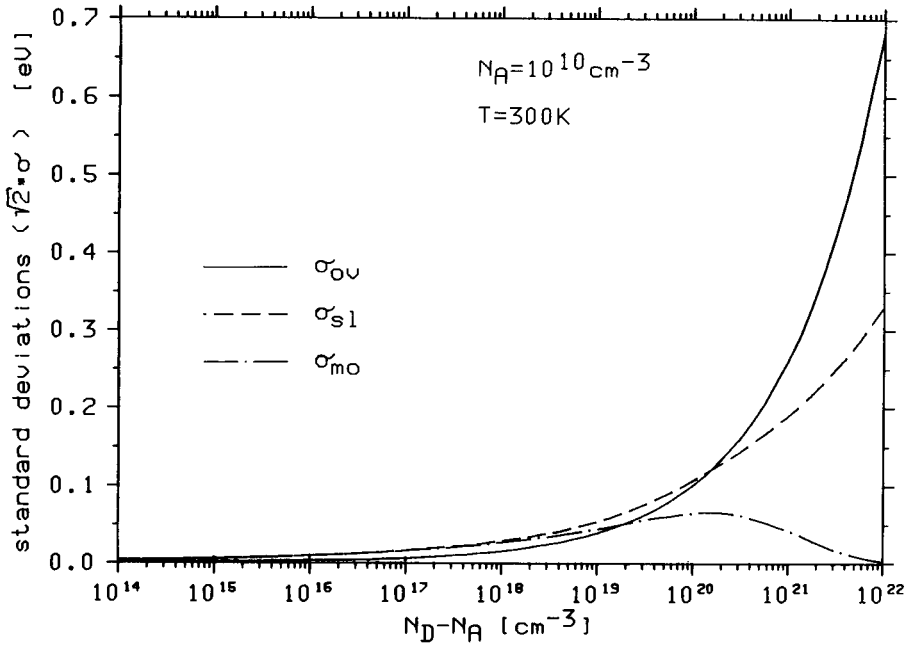

Fig. 13. Various standard deviations at 300 K for uncompensated n-silicon ($N_A = 10^{10}\,cm^{-3}$).

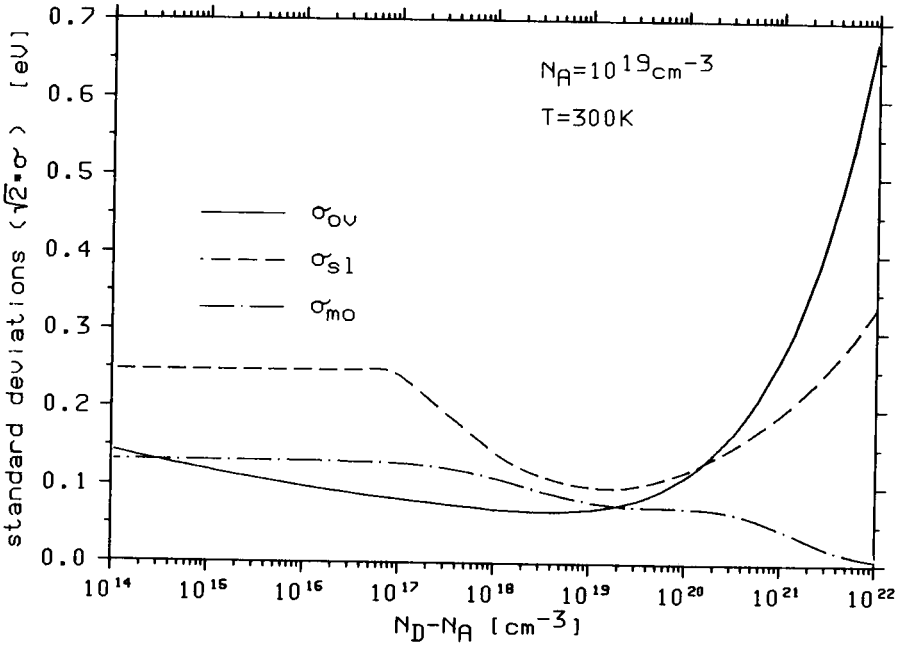

Fig. 14. Various standard deviations at 300 K for strongly compensated silicon ($N_A = 10^{19}\,cm^{-3}$).

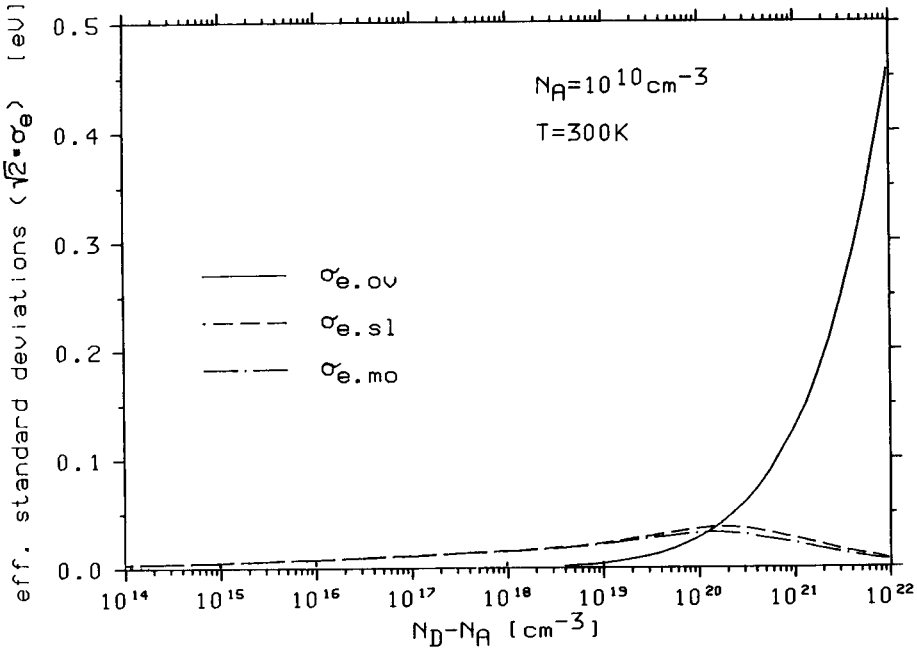

Fig. 15. Various effective standard deviations at 300 K for uncompensated n-silicon ($N_A = 10^{10}$ cm^{-3}).

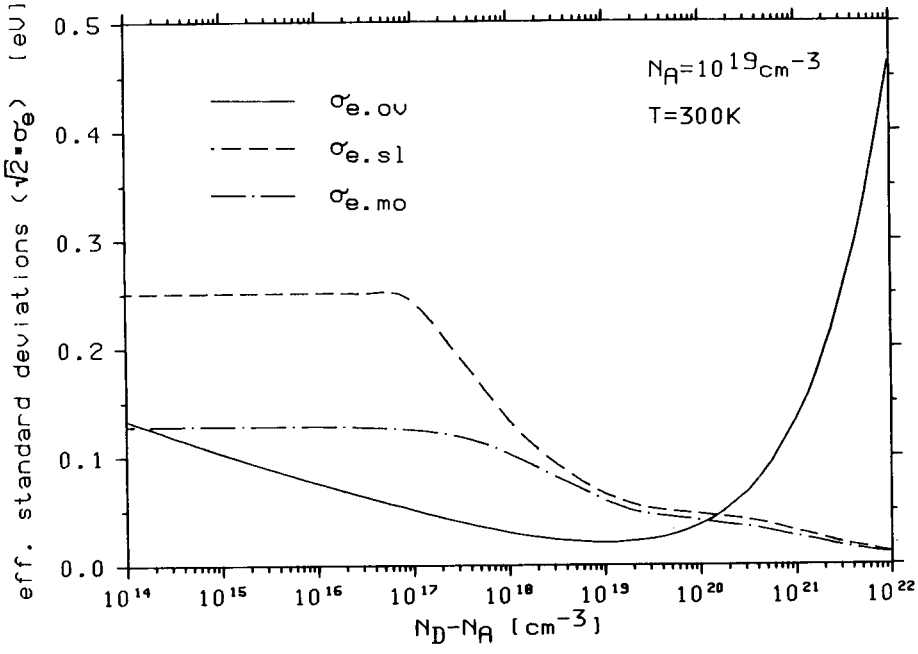

Fig. 16. Various effective standard deviations at 300 K for strongly compensated n-silicon ($N_A = 10^{19}$ cm^{-3}).

densities-of-states in silicon ($\sigma(N_A = N_D = N) > \sigma(N_D = 2N, N_A = 0)$. In the middle of Fig. 12 λ decreases with the number of the free carriers while the total impurity concentration increases slowly from $10^{19}\,cm^{-3}$ to $2\times10^{19}\,cm^{-3}$. If the degree of compensation decreases, the total number of impurity atoms increases weaker than the density of the free carriers. This leads to a better screening of the impurity atoms and the influence of the coulomb potentials on the densities-of-states gets weaker. The screening lengths, the standard deviation and the effective intrinsic number decrease monotonously (Figs. 12, 14 and 16). This effect is responsible for the descending shape of n_{ie} and for the minima. For very high doping concentrations the enormous number of impurity atoms disturb the band structure, though there would be enough free carriers to screen. Therefore, in the right part of Fig. 14 the increasing total impurity concentration exceeds the descending screening length and σ increases. σ_{mo} does not increase due to this rule because the factor $\exp(-0.5a/\lambda)$ diminishes σ_{mo} for small screening lengths.

6. COMPARISON OF CALCULATIONS TO MEASURED RESULTS

Figure 17 shows the measured values of the effective intrinsic number of Mertens et al. [19], Slotboom and De Graaf [1], Wieder [2] and Wulms [20] and our calculated results of the three models. Figure 17 shows that the three models do not differ very much for uncompensated material up to doping concentrations of

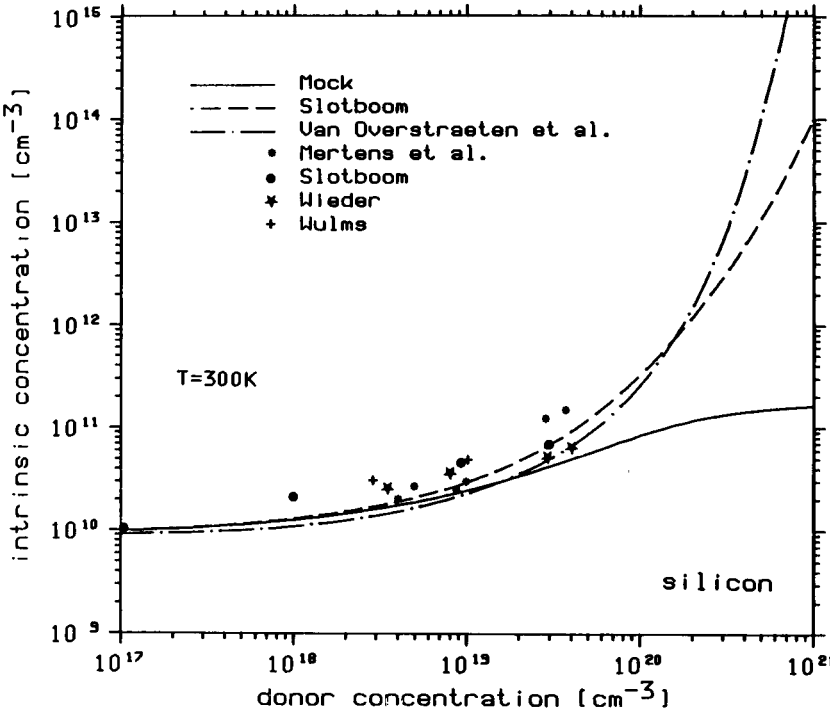

Fig. 17. Measured and calculated values for $(n_{ie}/n_{ie0})^2$ at 300 K for uncompensated silicon.

$5 \times 10^{19}\,\mathrm{cm}^{-3}$. As the measured values do not favour one of the models we cannot say which of the models describes the effective intrinsic number best.

In ref. [1] similar measurements and calculations have been examined for *npn*-bipolar transistors. The results show the same characteristics as ours. Unfortunately, no measured values for n_{ie} at various temperatures for compensated silicon have been published so that we cannot favour one of the models or check if these models are able to describe highly doped silicon sufficiently enough.

7. VALIDITY RANGE OF BOLTZMANN STATISTICS

In this section we try to find out how these models can be simply implemented into existing programs using Boltzmann statistics. For 300 K we examine if the relations between n and F_n or p and F_p can be described by the classical formulae using a doping dependent effective intrinsic number. Therefore, we simulate a semiconductor in thermodynamic equilibrium and a lightly disturbed semiconductor. For the exact models we calculated for the thermodynamic equilibrium n_0, p_0 and F_0 and set $n_{ie0}^2 = n_0 p_0$. Then we calculated F'_{n0} and F'_{p0} using the classical formulae

$$n'_0 = 0.5(N_D - N_A) + (0.25(N_D - N_A)^2 + n_{ie0}^2)^{1/2}$$

$$p'_0 = 0.5(N_A - N_D) + (0.25(N_D - N_A)^2 + n_{ie0}^2)^{1/2}$$

$$F'_{n0} = kT \log(n'_0/n_{ie0})$$

$$F'_{p0} = kT \log(p'_0/n_{oe0})$$

F''_{n0} and F''_{p0} are calculated in the same way, using a well established formula for the doping dependent intrinsic number which has been proposed in [1] and [11].

$$n''_i(T) = 6.43 \times 10^{15} T^{1.5} \exp((4.07T^2/(T + 1108) - 6370)/T)$$

$$n''_{ie}(N, T) = n_i(T) \exp((52.2/T)(C + (C^2 + 0.5)^{0.5})$$

$$C = \log(N_D/10^{17}\,\mathrm{cm}^{-3})$$

Then we "disturb" the equilibrium slightly by increasing the Fermi level of the minorities to

$$F_{pi} = F_{p0} + kT \log(10^i)$$

and calculate n_i, p_i and F_{ni} on charge neutrality

$$n(F_{ni}) - p(F_{pi}) = N_D^+ - N_A^-$$

Using the classical formulae and the n_{ie0} of the thermodynamic equilibrium, F'_{ni} and F'_{pi} are calculated. The results of the calculations are plotted in Figs. 18–23 for 300 K and various acceptor concentrations. The solid lines (———) are the values of F_p, the dashed-dotted lines (–·–·–·–) show F'_p and the dashed lines (– – – –) show F''_p. The lowest lines are valid for the thermodynamic equilibrium, the second, third and fourth lines are valid for $i = 1$, 2 and 3, respectively. We admit that the assumption

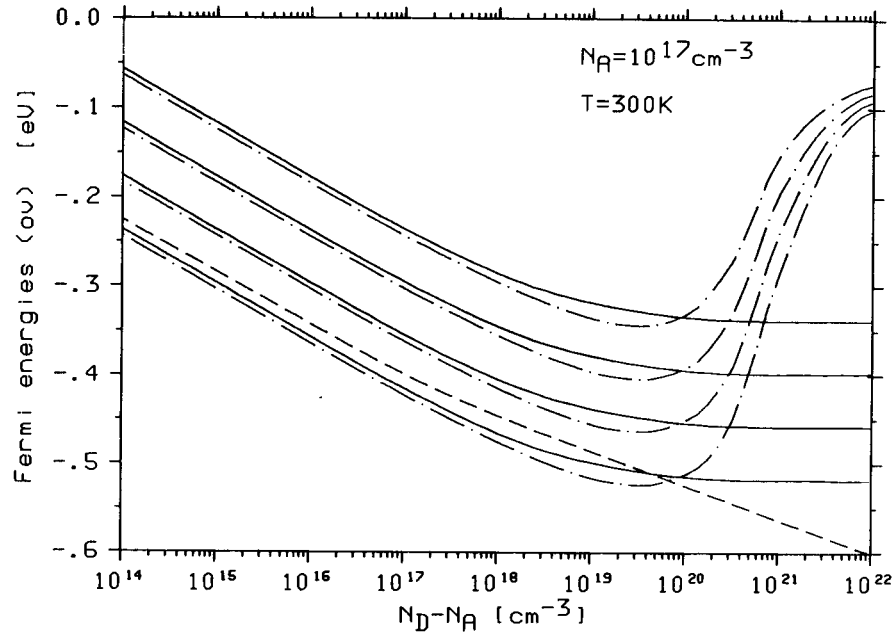

Fig. 18. Various Fermi levels, calculated by Van Overstraeten's model for n-doped silicon at 300 K.

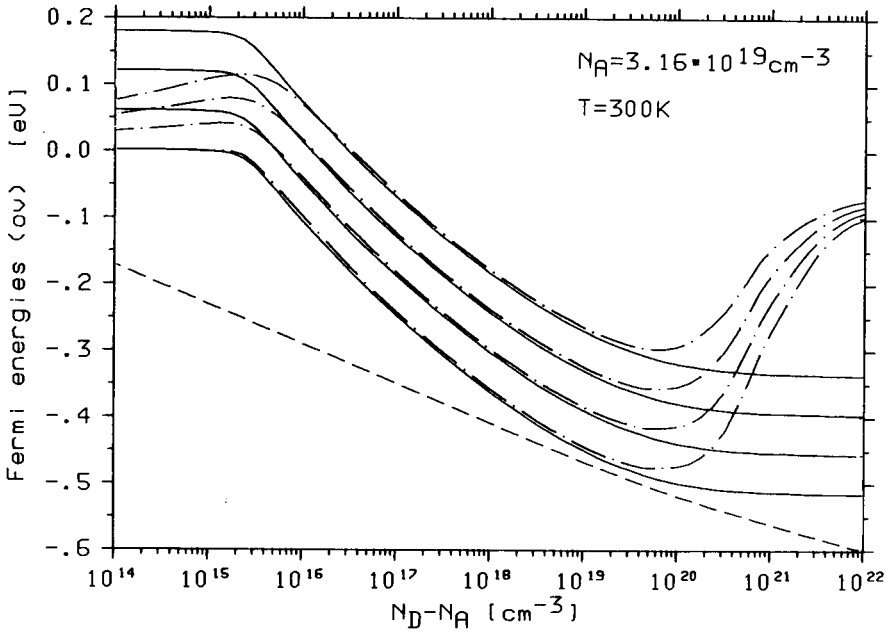

Fig. 19. Various Fermi levels, calculated by Van Overstraeten's model for n-doped silicon at 300 K.

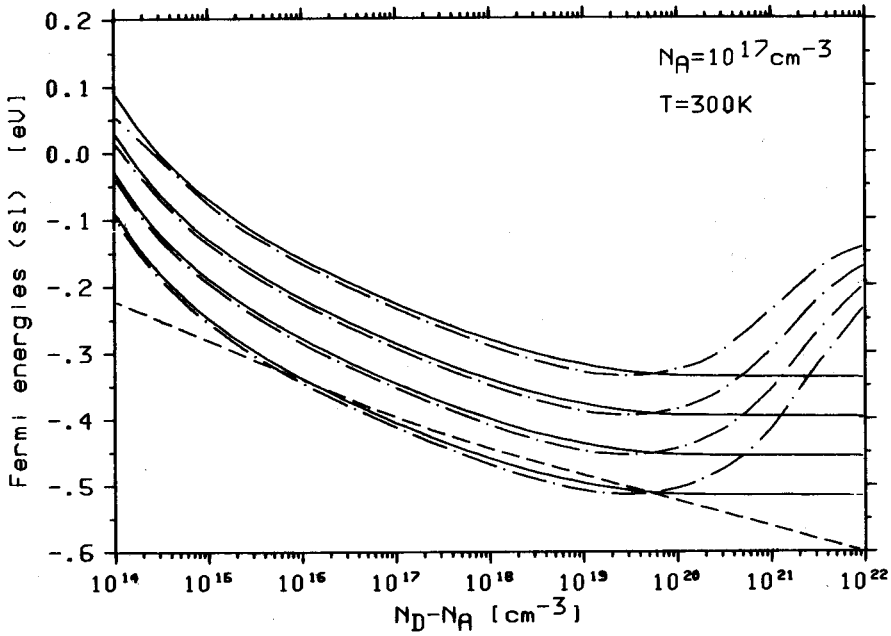

Fig. 20. Various Fermi levels, calculated by Slotboom's model for n-doped silicon at 300 K.

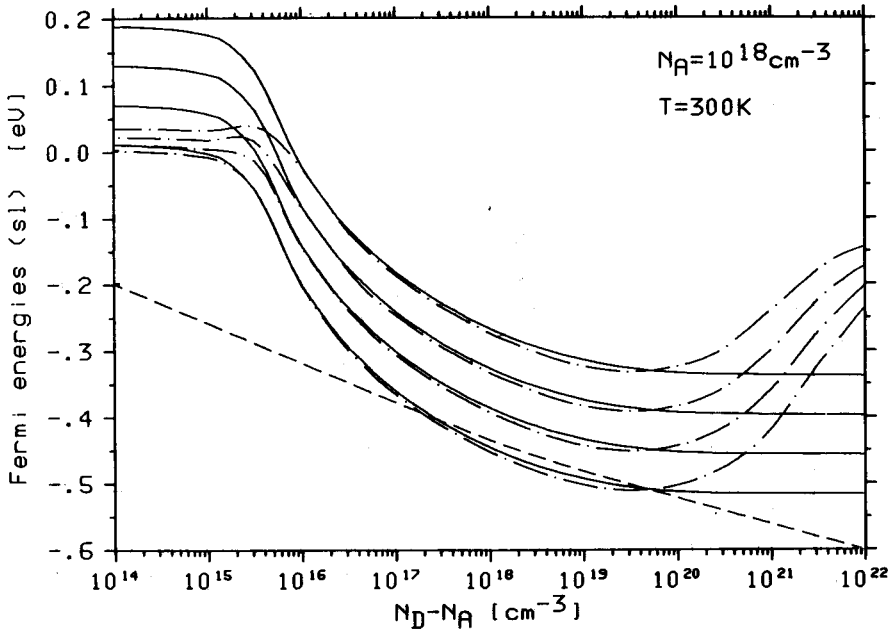

Fig. 21. Various Fermi levels, calculated by Slotboom's model for n-doped silicon at 300 K.

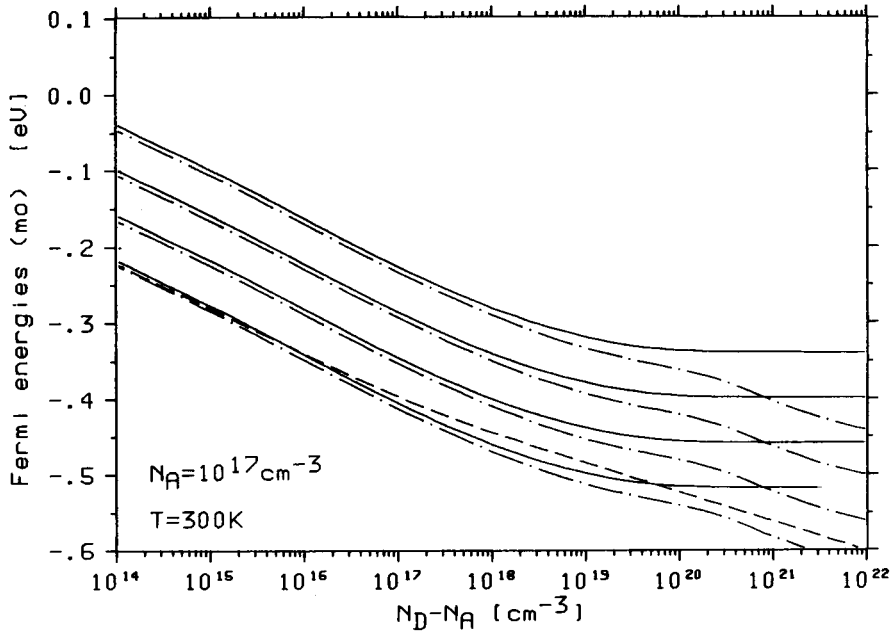

Fig. 22. Various Fermi levels, calculated by Mock's model in n-doped silicon at 300 K.

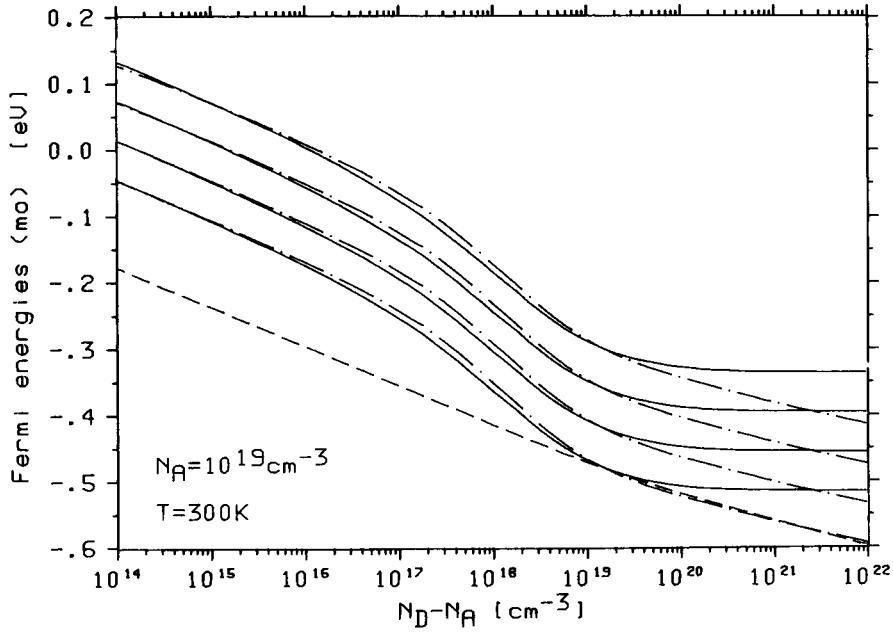

Fig. 23. Various Fermi levels, calculated by Mock's model for n-doped silicon at 300 K.

of a lightly disturbed semiconductor is only valid in the right part of Figs. 18–23; nevertheless, we have plotted the calculated results even when n equals approximately p. For low doping ranges F_p and F'_p show a small constant deviation caused by the difference of the relative masses of the electrons and the holes. This effect is taken into account by the theoretical models but neglected by the simple formulae of Boltzmann statistics.

The results of Van Overstraeten's model are plotted in Figs. 18 and 19. Figure 18 shows the results for low doped silicon. Up to doping concentrations of $9 \times 10^{19}\,\mathrm{cm}^{-3}$ the values of F_p and F'_p coincide for thermodynamic equilibrium as well as for the disturbed semiconductor.

Figure 19 shows the Fermi levels in strongly compensated silicon. Boltzmann statistics may be used up to doping concentrations of $7 \times 10^{19}\,\mathrm{cm}^{-3}$. In the left part of Fig. 19 it can be seen that Boltzmann statistics become more inaccurate the more the thermodynamic equilibrium is disturbed. F''_p coincides with F_p only when compensation is negligible.

Figures 20 and 21 show the results for Slotboom's model. The behaviour of F, F' and F'' is similar to the curves in Figs. 18 and 19. For very high doping concentrations n_{ie} increases strongly so that a small Fermi level is sufficient to cause an electron density n which fulfils charge neutrality.

Figures 22 and 23 show the results for Mock's model. The validity range of

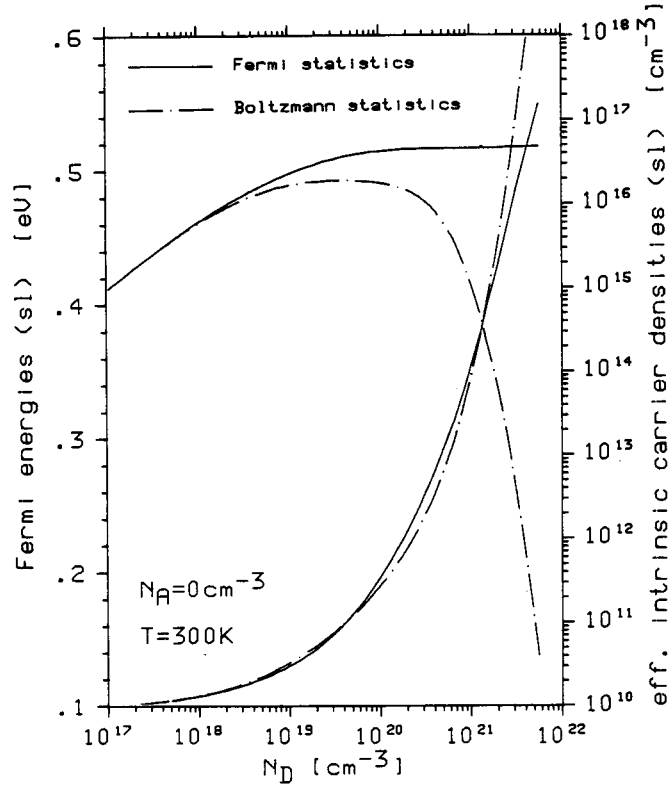

Fig. 24. Fermi levels and effective intrinsic carrier densities by Slotboom's model using Fermi statistics and Boltzmann statistics.

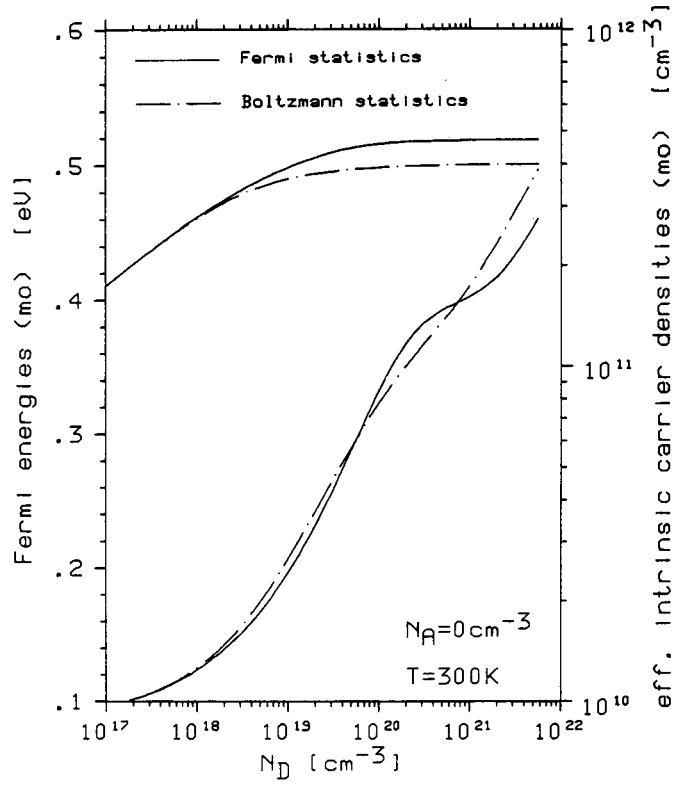

Fig. 25. Fermi levels and effective intrinsic carrier densities by Mock's model using Fermi statistics and Boltzmann statistics.

Boltzmann statistics is smaller; it ends for $N_A + N_D < 5 \times 10^{19}\,\mathrm{cm}^{-3}$. For high concentrations the behaviour of F_p differs from that of Van Overstraeten's model and Slotboom's model because the effective intrinsic number does not increase as strongly as $n_{ie,ov}$ or $n_{ie,sl}$.

At the end of this section we want to state that these densities-of-states models may only be used in connection with correct Fermi statistics. Boltzmann statistics lead to an overestimation of the densities-of-states especially when the Fermi level approaches the band edge. The results are too small Fermi levels and too large effective intrinsic numbers. These effects occur with increasing values of σ and σ_e and, therefore, are more drastic for Van Overstraetens's model than for Slotboom's model and have less influence on Mock's model.

Figures 24 and 25 show values of the Fermi energies and the n_{ie} for Slotboom's and Mock's models using Boltzmann statistics instead of Fermi statistics in eqs. (1) and (2). The Fermi energies show clearly the expected behaviour. The increase of n_{ie} in Slotboom's and Mock's theories is smaller than expected but is difficult to explain because the band structure depends on λ as a function of $\partial n/\partial F_n$ and $\partial p/\partial F_p$ and, therefore, on the distribution function itself. Figures 24 and 25 show that Boltzmann statistics must not be used for doping concentrations higher than $10^{18}\,\mathrm{cm}^{-3}$. The increase of n_{ie} in Van Overstraeten's model leads to such enormous values of n_{ie} that we have not plotted the calculated results.

8. FORMULAE FOR THE EFFECTIVE INTRINSIC NUMBER

For uncompensated material we offer temperature and doping dependent formulae for all three theories. The basis of these approximations are calculated values for a temperature range 275–400 K with a step width of 25 K and doping concentrations within the given validity ranges with a step factor of $\sqrt{10}$.

We define the structure of the formula for n_{ie} as

$$n_{ie} = \exp\left(a1(T) + a2(T)\left(\frac{N_D}{10^{17}\,\mathrm{cm}^{-3}}\right)^{a3(T)}\right)$$

and evaluate the coefficients by a least squares fit. We evaluate

$$a1(T) = -1.99765 \times 10^{+1} + 2.01814 \times 10^{-1} T - 1.97040 \times 10^{-4} T^2$$

for Van Overstraeten's model ($10^{15}\,\mathrm{cm}^{-3} < N_D < 10^{20}\,\mathrm{cm}^{-3}$)

$$a2(T) = +2.38838 \times 10^{-1} - 9.57814 \times 10^{-4} T + 1.07551 \times 10^{-6} T^2$$
$$a3(T) = +5.10190 \times 10^{-1} + 5.75190 \times 10^{-4} T - 7.01029 \times 10^{-7} T^2$$

for Slotboom's model ($10^{12}\,\mathrm{cm}^{-3} < N_D < 3.16 \times 10^{20}\,\mathrm{cm}^{-3}$)

$$a2(T) = +7.95811 \times 10^{-1} - 3.20439 \times 10^{-3} T + 3.54153 \times 10^{-6} T^2$$
$$a3(T) = +2.97104 \times 10^{-1} + 6.75707 \times 10^{-4} T - 4.90892 \times 10^{-7} T^2$$

and for Mock's model ($10^{12}\,\mathrm{cm}^{-3} < N_D < 10^{20}\,\mathrm{cm}^{-3}$)

$$a2(T) = +9.60563 \times 10^{-1} - 3.94127 \times 10^{-3} T + 4.41488 \times 10^{-6} T^2$$
$$a3(T) = +1.29363 \times 10^{-1} + 1.10709 \times 10^{-3} T - 9.56981 \times 10^{-7} T^2$$

The relative error is less than 10% for all theories within the defined doping ranges.

The formulae for Van Overstraeten's model which evaluate n_{ie} even for strongly compensated material are more difficult. After several attempts the following structure has given the best results for the temperature range 275–400 K.

$$n_{ie} = \exp(a_1 + \exp(a_2 + a_3 XS)) \exp(a_4 \exp(a_5 XS) \log(1.0 + \exp(a_6 + a_7 XD))$$

with

$$XS = \log((N_A + N_D)/10^{20}\,\mathrm{cm}^{-3}) \quad \text{and} \quad XD = \log((N_D - N_A)/10^{20}\,\mathrm{cm}^{-3})$$

The grid used as a basis for the approximation function is defined by $T = 275$ K, 300 K, 325 K, 350 K, 375 K and 400 K.

$$N_D - N_A = 10^{17}\,\mathrm{cm}^{-3},\ 3.16 \times 10^{17}\,\mathrm{cm}^{-3},\ 10^{18}\,\mathrm{cm}^{-3}, \ldots,\ 10^{21}\,\mathrm{cm}^{-3}$$

and

$$N_A = 10^{16}\,\mathrm{cm}^{-3},\ 1.78 \times 10^{16}\,\mathrm{cm}^{-3},\ 3.16 \times 10^{16}\,\mathrm{cm}^{-3},\ 5.62 \times 10^{16}\,\mathrm{cm}^{-3},$$
$$10^{17}\,\mathrm{cm}^{-3},\ 1.78 \times 10^{17}\,\mathrm{cm}^{-3}, \ldots,\ 10^{20}\,\mathrm{cm}^{-3}$$

The optimal coefficients have been evaluated by a least squares fit. Setting the temperature T in Kelvin the coefficients are defined by

$$a1(T) = -1.9966 \times 10^{+1} + 2.0248 \times 10^{-1} T - 1.9854 \times 10^{-4} T^2$$

$$a2(T) = +2.8494 \times 10^{+0} - 8.5734 \times 10^{-3} T + 6.7176 \times 10^{-6} T^2$$

$$a3(T) = +1.1223 \times 10^{+0} + 3.1987 \times 10^{-3} T - 4.9961 \times 10^{-6} T^2$$

$$a4(T) = +2.4212 \times 10^{+1} - 1.7740 \times 10^{-1} T + 4.6916 \times 10^{-4} T^2 - 4.2766 \times 10^{-7} T^3$$

$$a5(T) = +1.5175 \times 10^{+0} + 1.3427 \times 10^{-3} T$$

$$a6(T) = -2.1691 \times 10^{+0} + 2.4694 \times 10^{-2} T - 8.9726 \times 10^{-5} T^2 + 9.7262 \times 10^{-8} T^3$$

$$a7(T) = +1.1152 \times 10^{+1} - 1.0839 \times 10^{-1} T + 3.1002 \times 10^{-4} T^2 - 2.9810 \times 10^{-7} T^3$$

The relative error of n_{ie} is less than 20% for the temperature and the doping range.

The following formulae describe the effective, intrinsic carrier densities calculated by Van Overstraeten's model in the temperature range 1073–1473 K:

$$n_{ie} = \exp(a_1 + a_2 XM + a_3 XD + a_4 XDXM) + \exp(a_6 + a_7 XS) + \exp(a_8 + a_9 XS)$$

with

$$XS = \log((N_D + N_A)/10^{20}\ \mathrm{cm}^{-3})$$

$$XM = \log(N_A/10^{20}\ \mathrm{cm}^{-3})$$

and

$$XD = \log((N_D - N_A)/10^{20}\ \mathrm{cm}^{-3})$$

The grid used for the calculation of the coefficients is defined by $T = 1073$ K, 1173 K, 1273 K, 1373 K and 1473 K.

$$N_D - N_A = 10^{17}\ \mathrm{cm}^{-3},\ 3.16 \times 10^{17}\ \mathrm{cm}^{-3},\ 10^{18}\ \mathrm{cm}^{-3}, \ldots,\ 10^{22}\ \mathrm{cm}^{-3}$$

and

$$N_A = 10^{17}\ \mathrm{cm}^{-3},\ 1.78 \times 10^{17}\ \mathrm{cm}^{-3},\ 3.16 \times 10^{17}\ \mathrm{cm}^{-3},\ 5.62 \times 10^{17}\ \mathrm{cm}^{-3},\ 10^{18}\ \mathrm{cm}^{-3}, \ldots,\ 3.16 \times 10^{21}\ \mathrm{cm}^{-3}$$

The coefficients can be evaluated by the following formulae setting the temperature T in Kelvin:

$$a1(T) = +3.8217 \times 10^{+1} + 3.0973 \times 10^{-3} T$$

$$a2(T) = +1.0476 \times 10^{+1} - 7.8184 \times 10^{-3} T + 2.2944 \times 10^{-6} T^2$$

$$a3(T) = -1.8513 \times 10^{+0} + 1.6397 \times 10^{-3} T - 4.8164 \times 10^{-7} T^2$$

$$a4(T) = +8.4264 \times 10^{-1} - 8.2597 \times 10^{-4} T + 2.6367 \times 10^{-7} T^2$$

$$a5(T) = +3.5449 \times 10^{+1} + 6.0164 \times 10^{-3} T$$

$$a6(T) = +1.8134 \times 10^{+0} - 2.8084 \times 10^{-3} T + 3.2965 \times 10^{-7} T^2$$

$$a7(T) = -6.1859 \times 10^{-1} + 2.2840 \times 10^{-3} T - 6.4366 \times 10^{-7} T^2$$

$$a8(T) = +3.2140 \times 10^{+0} + 6.2687 \times 10^{-3} T$$

$$a9(T) = +1.0109 \times 10^{+1} - 7.0976 \times 10^{-3} T + 1.5504 \times 10^{-6} T^2$$

The relative error of the n_{ie} is less than 15% for the temperature and doping range.

9. CONCLUSIONS

The calculated values of the effective intrinsic number show that at 300 K the theories differ widely when the doping concentration increases over $3 \times 10^{19}\,\mathrm{cm}^{-3}$ or when strongly compensated material is present.

Comparison of the calculated and measured values shows that neither for n-doped nor for p-doped silicon the theories describe the effective intrinsic number sufficiently well.

The measured values do not favour any of the models; therefore, we cannot say which model describes n_{ie} best. In order to give a better judgement of the three models, measurements of very high doped or strongly compensated silicon should be performed.

The calculations show that Boltzmann statistics are valid when the total doping concentration is less than $5 \ldots 10 \times 10^{19}\,\mathrm{cm}^{-3}$. Up to these concentration limits Boltzmann statistics can be applied if the doping dependence is considered either by an effective intrinsic number or by a doping dependent bandgap.

We believe that these concentration limits can also be applied to formulae which have been derived by approximations of measured values of n_{ie}. For doping concentrations up to $5 \ldots 10 \times 10^{19}\,\mathrm{cm}^{-3}$ it is possible to implement formulae derived from measurements of these complicated theories into simulation programs considering a doping dependent effective intrinsic number and Boltzmann statistics. We are afraid that for higher doping concentrations there is no escape from using more complicated theories which take into account Fermi statistics and a sophisticated model of the highly doped silicon.

APPENDIX A

The calculation of n and $\partial n/\partial F_n$ as a function of T, N_A, N_D, F_n and λ with a relative error less than 1%:

The Fermi function

$$f(E) = \frac{1}{1 + \exp((E - F_n)/kT)}$$

the densities of states of silicon

$$\rho_c = C_c y \frac{(E - E_G/2)}{\sqrt{2}\sigma}$$

and the densities of states of the impurity atoms

$$\rho_D = C_D \exp\left(-\frac{(E - E_D)^2}{2\sigma_e^2}\right)$$

can be reduced by the linear transformations $x = (E - F_n)/kT$, $x = (E - E_G/2)/\sqrt{2}\sigma$ and $x = (E - E_D)/\sqrt{2}\sigma_e$ to dimensionless functions $f(x) = 1/(1 + \exp(x))$, $\rho_C(x) = C_c y(x)$ and $\rho_D = C_D \exp(-x^2)$ which are independent from the physical values of E_D, E_G, T and F_n. These reduced functions are approximated piecewise by functions $g(x)$ so that the relative error is less than 0.5%. The functions $g(x)$ have the property that the integrals $\int \rho(E) f(E)\,dE$ and $\int \partial f(E)/\partial F_n \rho(E)\,dE$ can be integrated exactly within the intervals. The multiplication doubles the relative error to 1%, the addition of the values of n and $\partial n/\partial F_n$ calculated within the intervals does not affect the relative error any more. We have defined

$$g_i(x) = \sum_{j=1}^{i} c_{ij} \exp(-a_{ij}^2 x^2 - b_{ij} x)$$

The functions $y(x)$ and $f(x)$ can easily be approximated by functions $g_f(x)$ and $g_y(x)$. The coefficients a_{ij}, b_{ij} and c_{ij} are evaluated by least squares fit. As an example we give our approximation of the Fermi function $f(x)$

$$\begin{aligned} f(x) = 1/(1 + \exp(x)) = {} & +0.256538 \exp(-(0.2157410x)^2 - 0.5x) \\ & +0.241270 \exp(-(0.4378350x)^2 - 0.5x) \end{aligned}$$

This approximation is valid for $-4.89 < x < +4.89$. It permits a simple evaluation of n as well as of $\partial n/\partial F_n$ which is necessary for the Newton iterations in F and for the evaluation of the screening length in Slotboom's and Mock's models.

We should like to remark that even the partial derivatives of the carrier densities with respect to the temperature can be evaluated by this method.

APPENDIX B

The fixpoint iteration of Aitken:

For Slotboom's or Mock's model we have to find a value for the screening length λ

so that for charge neutrality

$$\lambda_1 = \lambda_1(N_D, N_A, \partial n/\partial F_n, \partial p/\partial F_p, \lambda_0) = \lambda_0$$

where λ_0 is the value used as the input parameter in the function $n(T, N_A, N_D, F_n, \lambda_0)$ and λ_1 is the value which is evaluated by eq. (5 sl) or (5 mo). The simple Banach fixpoint iteration

$$\lambda_1 = \Phi(\lambda_0)$$

converges only for high temperatures. In order to have a program for all temperature ranges we have implemented the improved Aitken fixpoint iterations. We have calculated λ_1 and λ_2 by two Banach iterations

$$\lambda_1 = \Phi(\lambda_0) \quad \text{and} \quad \lambda_2 = \Phi(\lambda_1)$$

and define

$$\lambda_3 := \lambda_0 + (\lambda_1 - \lambda_0)/(1 - (\lambda_2 - \lambda_1)/(\lambda_1 - \lambda_0))$$

λ_3 should be a better value for λ than λ_0. Therefore, $\lambda_4 = \Phi(\lambda_3)$ is evaluated.
If $[\lambda_3 - \lambda_4] < \lambda_4 \times 10^{-5}$ we stop the iteration, otherwise we set

$$\lambda_0 := \lambda_3 \quad \text{and} \quad \lambda_1 := \lambda_4$$

and continue until the iteration converges. The calculation has shown that these iterations converge for all temperatures and concentration ranges which have been used for this article.

REFERENCES

[1] J.W. Slotboom and H.C. De Graaf, Measurements of bandgap narrowing in Si bipolar transistors, Solid-St. Electron. 19 (1976) 857–862.
[2] A.W. Wieder, Emitter effects in shallow bipolar devices, IEEE Trans. Electron Devices ED-27 (8) (1980) 1402–1408.
[3] R. Mertens and R. Van Overstraeten, Measurements of the minority carrier transport parameters in heavily doped silicon, IEEE, IEDM (1978) 320–323.
[4] F.A. Lindholm, A. Neugroschel, C.T. Sah, M.P. Godlewski and H.W. Braudhorst, A methodology for experimentally based Determination of gap shrinkage and effective lifetimes in the emitter and base of *p–n* junction solar cells and other *p–n* junction devices, IEEE Trans. Electron Devices ED-24 (1977) 402–410.
[5] G.E. Possin, M.S. Adler and B.J. Baliga, Measurements of bandgap narrowing in heavily doped epitaxial emitters and the modeling of heavily doped silicon, IEEE, IEDM (1980) 270–275.
[6] V.L. Bonch-Bruevich, The electronic theory of Heavily Doped semiconductors (Elsevier, Amsterdam, 1969).
[7] T.N. Morgan, Broadening of impurity bands in heavily doped semiconductors, Phys. Rev. 139 (1965) A343–A348.
[8] E.O. Kane, Thomas–Fermi approach to impure semiconductor band structure, Phys. Rev. 131 (1963) 79–88.
[9] R.J. Van Overstraeten, H.J. De Man and R.P. Mertens, Transport equations in heavy doped silicon, IEEE Trans. Electron Devices, ED-20 (3) (1973) 290–298.

[10] R.K. Jain and R.J. Van Overstraeten, Theoretical calculations of the Fermi level and of other parameters in phosphorus doped silicon at diffusion temperatures, IEEE Trans. Electron Devices, ED-21 (2) (1974) 155–165.
[11] J.W. Slotboom, The *pn*-product in silicon, Solid-St. Electron. 20 (1977) 279–283.
[12] M.S. Mock, Transport equations in heavily doped silicon and the current gain of a bipolar transistor, Solid-St. Electron. 16 (1973) 1251–1259.
[13] A. Nakagawa, One-dimensional device model of the *npn* bipolar transistor including heavy doping effects under Fermi statistics, Solid-St. Electron. 22 (1979) 943–949.
[14] B.S. Polsky and J.S. Rimshans, Two-dimensional numerical simulation of bipolar semiconductor devices taking into account heavy doping effects and Fermi statistics, Solid-St. Electron. 26 (4) (1983) 275–279.
[15] F.J. Morin and J.P. Maita, Electrical properties of silicon containing arsenic and boron, Phys. Rev. 96 (1954) 28–35.
[16] D.D. Kleppinger and F.A. Lindholm, Impurity concentration dependent density of states and resulting Fermi level for silicon, Solid-St. Electron. 14 (1971) 407–416.
[17] F.H. Gaensslen and R.C. Jaeger, Temperature dependent threshold behaviour of depletion mode mosfets, Solid-St. Electron. 22 (1979) 423–430.
[18] W. Jüngling, Hochdotierungseffekte in Silzium, Diplomarbeit am Institut für Allgemeine Elektrotechnik und Elektronik, Abteilung für Physikalische Elektronik, TU-Wien, May 1983.
[19] R. Mertens, J. Meerbergen, J. Nijs and R. Van Overstraeten, Measurements of the minorit-carrier transport Parameters in heavily doped silicon, IEEE Trans. Electron Devices, ED-27 (5) (1980) 949–955.
[20] H. Wulms, Base current of I^2L transistors, IEEE J. of Solid-St. Circuits 12 (2) (1977) 143–150.